Mechanical and Thermal Properties of Copper Inverse Opals for Two-Phase Convection Enhancement

Yoonjin Won, Michael T. Barako, Damena D. Agonafer, Mehdi Asheghi, and Kenneth E. Goodson
Department of Mechanical Engineering
Stanford University
Stanford, California 94305
Email: yoonjin@stanford.edu

ABSTRACT

Nanoengineered structures have received significant attention due to the application of porous media convection structures. Metal porous structures provide unique combinations of large surface to volume ratio, high conductivity, and mechanical compliance. The integration of metal porous structures can improve the performance of convective heat exchangers for high heat flux thermal management. Copper inverse opals (CIOs) are more attractive because their geometry can be precisely controlled and determined at the pore level. This study reports a combination of experiments, simulations, and analytical models to understand the mechanical and thermal properties of CIOs coupled with structural information. Detailed image analysis to quantify the porosity and pore geometry is followed. The mechanical modulus and thermal conductivity of CIOs show a strong dependence on the porosity. The mechanical compliance of 20-50 GPa and high thermal conductivity of ~100 W/mK are promising for a variety of applications including microchannels applications.

KEY WORDS: porous structures, inverse opal, modulus, thermal conductivity, nanoengineered structures.

NOMENCLATURE

A	cross-sectional area of a beam, m^2
E	Young's modulus, GPa
I	the second moment of area, m^4
L	length, m
V	volume, m^3
d	diameter, m
f	resonant frequency, Hz
k	thermal conductivity, W/m-K
q''	heat flux, W/m^2
t	thickness, m

Greek symbols

Δ	resonant frequency shift to the original resonant frequency
κ	thermal conductivity ratio of the solid to the fluid
ρ	mass density (kg/m^3)
ν	poisson's ratio
ϕ	porosity

Subscripts

b	beam
eff	effective
n	neck
NF	nanostructured film
p	pore
s	solid
Si	silicon
shell	shell
unit	unit cell

INTRODUCTION

The capability of high-power electronic systems leads to a corresponding need for high power density cooling. Since the first demonstration by Tuckerman and Pease [1], there has been much work on single- and two-phase cooling. As the power density increases, single-phase liquid cooling becomes inefficient due to pumping power requirements. Two-phase liquid cooling is more appropriate to reduce the pumping power but suffers from bubble instabilities, flow regime oscillation, and dryout regions [2]-[4]. Nanoengineered structures and surfaces that can be integrated into liquid-vapor phase change systems have revolutionized the design of heat sinks [5], [6]. Porous structures show outstanding combinations of large surface to volume ratio, high conductivity, and mechanical compliance. Once liquid is pumped into these porous structures, they can be contained therein by capillary forces [7]. These ultra-thin evaporating liquid films in porous structures improve heat dissipation and decrease the total thermal resistance of the system. In addition, nano-structures allow the vapor phase to discharge via nanoscale pores; this effectively separates the vapor and liquid phases. David *et al*. [8] demonstrated vapor removal through a porous hydrophobic membrane, which decreased the pressure drop during flow boiling in microchannels. There are several nanostructures to mimic superhydrophobic surfaces to manipulate their wetting properties [9]-[12]. Therefore, nanostructured surfaces are designed to control fluidic behavior and enhance heat dissipation in microfluidic systems.

Nanoporous surfaces can provide novel liquid-vapor heat exchange augmented by the phase change as a high heat flux thermal management solution. They are often employed in fluidic systems to improve the two-phase cooling systems [8], [13]. The integration of metal porous structures can improve the performance of convective heat exchangers due to the high thermal conductivity and small hydraulic diameter. In order to understand the performance of this porous film, it is critical to have precisely controlled structures. Here, we propose to use copper inverse opals (CIOs) as wicking structures, which have the advantage of precise control over pore sizes and distribution. To utilize them in applications, it is important to characterize the mechanical modulus and thermal conductivity of those structures, both of which are functions of porosity. We adopt a microfabricated resonator

technique [14], which measured the mechanical properties of various nanostructured materials in past, including carbon nanotube arrays, nanowire films, and thin metal layers [14]-[16]. In addition, we develop COMSOL Multiphysics simulations to estimate the mechanical modulus and thermal conductivity as a function of porosity. The simulations are consistent with much simpler models. Thus, combined experimental, analytical, and computational techniques applied to the CIOs are presented in this paper.

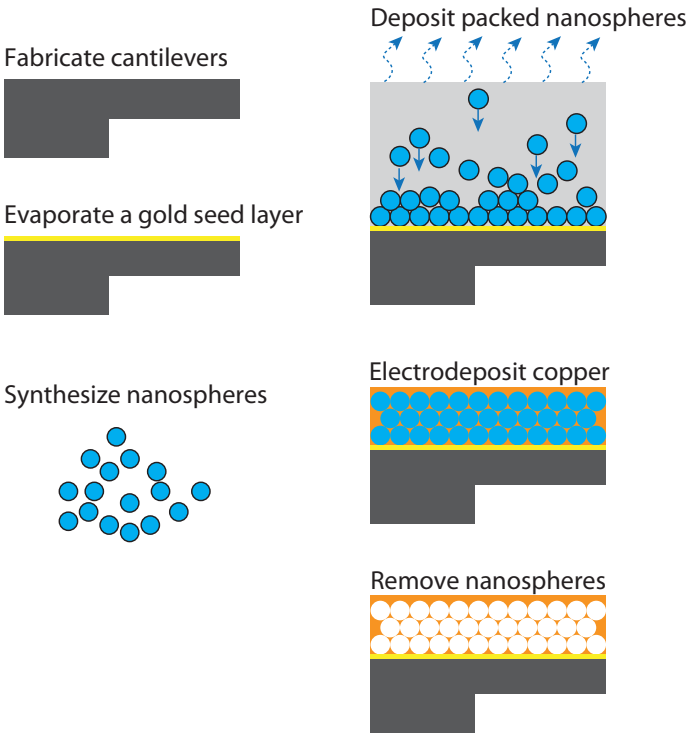

Fig.1 Fabrication procedure of copper inverse opal structures. Synthesized nanospheres are deposited on a surface with an electrode seed layer. The interstitial spaces between the nanospheres are filled with electrodeposited copper. The nanospheres are then removed by wet etching, which leaves periodically porous voids in the copper film.

INVERSE OPAL STRUCTURE FABRICATION

The porous copper films are engineered on target substrates using a drop casting method (Fig. 1) [17], [18]. Silica nanospheres with 675 nm diameters are chemically synthesized using the Stöber process [19]-[21]. The nanospheres are then functionalized with 3-aminopropyl (diethoxy) methylsilane (Sigma-Aldrich) to prevent sphere aggregation. A 5 nm-thick titanium adhesion layer and 100 nm-thick gold layer are evaporated on the target substrate, which can be connected with the working electrode during the electrodeposition process. The nanospheres are deposited in methanol suspension in increments of 5 µL/drop at room temperature, and they are self-assembled during solvent evaporation into a close-packed structure on the surfaces by heating the substrate to 80°C. By repeating the drop casting step, the height of the colloidal crystal (corresponding to the nanosphere template thickness) is increased to a thickness greater than 10 µm. Copper is then electrodeposited potentiostatically into the interstitial spaces of the nanospheres. The copper film thickness is controlled by the time of electrodeposition because the growth rate is approximately linear with time. At the deposition overpotential used in this work (V = -200 mV vs. Ag/AgCl), 10 mins of electrodeposition results in the film thickness of 3.6 µm. The actual film thickness is confirmed by taking cross-sectional SEMs. Subsequently, the nanospheres are dissolved in an aqueous solution of 2-5% HF at room temperature for 45 minutes. This reveals a copper structure on the surface of the cantilever with the inverse geometry of the initial close-packed spheres, which is known as an inverse opal. This method is advantageous because it is possible to vary the diameter of the nanospheres in each layer to change the porosity of the template. The details of the fabrication process of CIOs are explained in [22]. In this work, CIOs with a thickness ranging from 3 to 7 microns and pore sizes of 675 nm are grown directly on the cantilevers and substrates. The actual CIOs are shown in Fig. 2.

The image analysis is followed to characterize the porosity (ϕ) and permeability of CIOs as well as to provide input to the simulations. Image analysis estimates the average of pore diameter (d_p) of CIOs to detect morphological variations. By expecting that face centered cubic (FCC) structures from our growth process [24], we use a unit cell volume approach of an FCC structure (Fig. 3a). Here, the void fraction (=ϕ) is the ratio of interior volume of spheres equal to $n \times V_p$) to the volume of a unit cell (V_u). Here we define pore diameter, neck diameter, shell thickness, and number of spheres of a unit cell as d_p, d_n, t_s, and n, respectively. Thus, the pore radius and neck radius are r_p and r_n. In the case of an FCC crystal, n=4 (=1+6x0.5). The interior

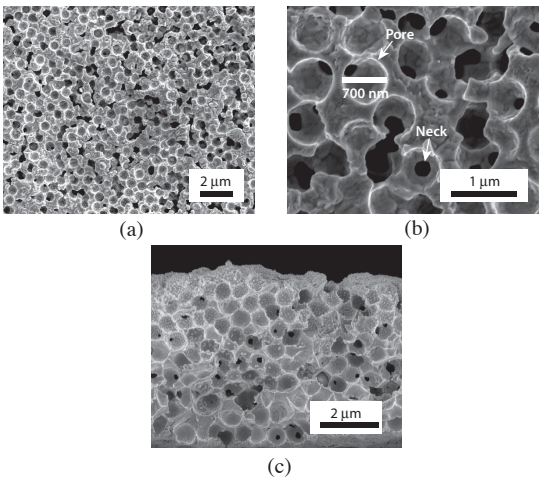

Fig.2 CIOs on a microfabricated resonator. (a) The top view of CIOs. (b) The pore size is a diameter of 675 nm, and thickness of this film is 3.6 µm. (c) The cross-sectional view of CIOs.

volume of spheres is

$$n \cdot V_p = \frac{16}{3}\pi r_p^3 \cdot \quad (1)$$

The unit cell volume is

$$V_u = A^3 \quad (2)$$

where

$$A = 2\sqrt{2}B \quad (3)$$

$$B = \left(\left(r_p + t_s\right)^2 - r_n^2\right)^2 \cdot \quad (4)$$

Pore diameter and shell thickness between spheres from the image analysis are plugged back to the Eq. (1) and (4) to calculate the porosity. Since the purpose of our structure is to provide the flow path, it is important to understand the permeability of our films. This means that it is also critical to investigate how the spheres are contacting well. The contacts formed between the spheres are referred to as necks. All images of the film are taken using an FEI XL30 Sirion scanning electron microscope (SEM). The process starts with cropping the SEM images and binaries to convert grey image to black and white images. The black and white images are then inverted for the subsequent morphological processing. The morphological processing of erosion and dilation is performed to remove small objects from an image while preserving the shape and size of larger objects in the image. Post-processing filters out small or large segments, which may reflect combined pores or noises. The intersections between the pores and 50 evenly spaced probe lines are counted in both the horizontal and vertical directions to compute t_s. An example of the final binary image is shown in Fig. 3b. Image analysis reveals that the structures have a porosity of 50% and pore size of 675 nm.

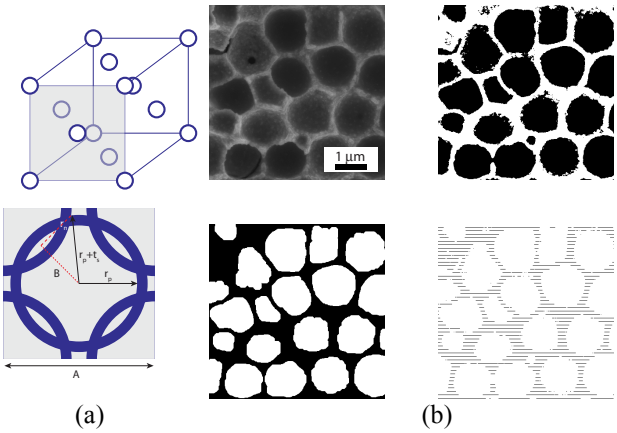

(a) (b)

Fig.3 (a) A three-dimensional diagram containing a face centered cubic. (b) An example of the actual SEM image, binary image, final image, and image with probe lines after the morphological processing.

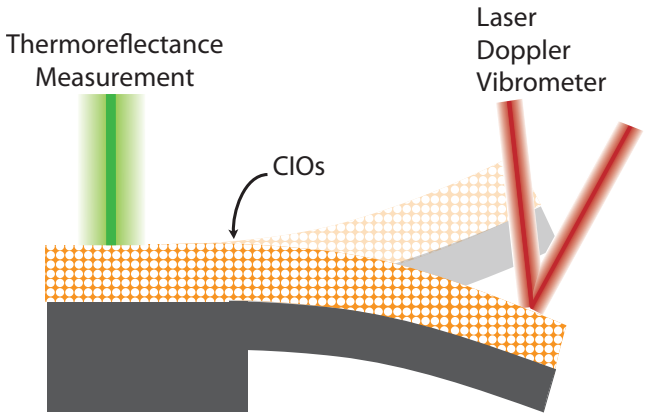

Fig.4 Resonant-based mechanical characterization technique using a laser Doppler vibrometer [14]. Resonators are used as diving boards to capture the mechanical modulus of nanostructured materials. This sample can often be combined with our thermoreflectance measurement for thermal characterization [23].

Table.1 Resulting parameters using image analysis for an example image.

Parameter	Value
d_p	675 nm
STD of d_p	68 nm
t_s	60 nm
d_n	50 nm
STD of d_n	10 nm

MECHANICAL CHARACTERIZATION

The nanoporous structures are often grown onto the surfaces and into the channels of electronic and microfluidic devices. The mechanical compliance of these nanostructured films makes them promising to accommodate thermal expansion mismatch at the interface between two dissimilar materials. It is therefore critical to undertand the mechanical responses of nanostructures.

Resonator Technique

The mechanical modulus of porous structures is measured using microfabricated resonator technique and a laser Doppler vibrometer (LDV), as shown in Fig. 4. An LDV (Polytec OFV 2500) captures the resonant frequency shift of resonator with and without the CIOs on a resonator. Based on composite beam theory, we calculate the effective moduli of CIOs. The effective modulus of nanostructured film is expressed as

$$E_{NF,eff} = \frac{E_{Si}}{I_{NF}}\left(\left(1 + \frac{\rho_{NF,eff} A_{NF}}{\rho_{Si} A_{Si}}\right) \cdot \left(1+\Delta\right)^2 I_{Si,0} - I_{Si}\right) \quad (5)$$

where E, I, ρ, and A, are respectively the modulus, the second moment of area, density, and cross-sectional area of the beam. The subscripts, *Si,0*, *Si*, and *NF* denote the silicon layer of a silicon-only cantilever, the silicon, and nanostructured film of CIOs of a composite cantilever, respectively. The resonant frequency shift Δ is the ratio of with the composite beam to the original resonant frequency of

the silicon beam. The detailed analysis and fabrication process are described in the literature [14]. We extract the modulus of 3.6 and 7.2 μm-thick films, which are indicated in Fig. 6.

COMSOL model

We develop a finite element method (FEM) model using COMSOL Multiphysics to represent the geometry and deformation of the CIOs on cantilevers. The beam is fixed at one end and free at the other, as shown in Fig. 5. At the fixed end of the beam, because no displacement or rotation of the beam is produced, the deflection and slope at the left end (x = 0) are zero. Since no external bending moment is applied at the free end of the beam (x = L), the bending moment at that location is zero. In addition, if there is no external force applied to the beam, the shear force at the free end is also zero. Thus, using these boundary conditions and solving the one-dimensional Euler-Bernoulli differential equation, the resonant frequencies of a fixed-free beam can be calculated. The single porous beam (Fig. 5) has spherical voids. The void of pores is air, and the solid matrix is copper. The porosity is calculated by the ratio of the void volume to the total volume. By varing the pore diameters from 8-10 μm, this model has the range of porosity of 25-50%. For a single porous beam, the resonant frequency for given dimensions is obtained. The resonant frequency is used to extract the effective modulus:

$$E_{NF,eff} = \left(\frac{2\pi f}{1.015}\frac{L_b^2}{t_b}\right)^2 \rho_{NF,eff} \qquad (6)$$

where t_b, L_b, and f is the thickness, length of a beam, and resonant frequency, respectively. $E_{NF,eff}$ and $\rho_{NF,eff}$ are the effective mododulus and effective density of the beam with spherecial pores.

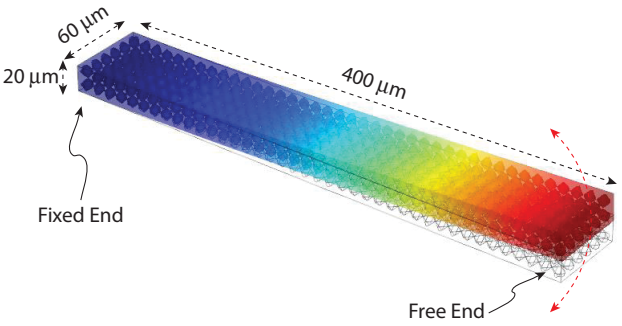

Fig.5 COMSOL Multiphysics model for the mechanical characterization. The obtained resonant frequency (f) from the simulation is used to calculate the effective modulus ($E_{NF,eff}$) of the beam with spherical pores.

Porosity Effect on the Modulus of CIOs

The elastic properties of porous materials are decided by the porosity of nanostructures [25], [26]. Therefore, it is important to investigate the correlation between the porosity and modulus of porous structures. Past studies show several approaches to decide property-porosity relations for porous materials. The elastic properties of porous materials over an entire porosity range can be generally expressed to the power-law empirical relationship by

$$\frac{E_{NF,eff}}{E_s} = \left(1 - \frac{p}{p_c}\right)^C \qquad (7)$$

where $E_{NF,eff}$ is the effective Young's modulus of porous material with a porosity of p, E_s is Young's modulus with a zero-porosity, and p_c is the porosity at which the effective Young's modulus becomes zero, which is often one. In Eq. (4), C is an emphirical parameter, and this can be determined by porosity, pore shapes and size, etc. For example, Coble and Kingery explained the properties of porous alumina as a function of porosity. Roberts and Garboczi provided the modulus prediction of ceramic as a function of pore size and structures by comparing with FEM models. Thus, the upper bound and lower bound of the estimation are decided by using C=1.1 and 2. The predicted lines are indicated in Fig. 6. Both equations qualitatively agree with the trend of decreasing modulus with porosity. The predicted equation (C=1.1) shows a very good agreement with the COMSOL results.

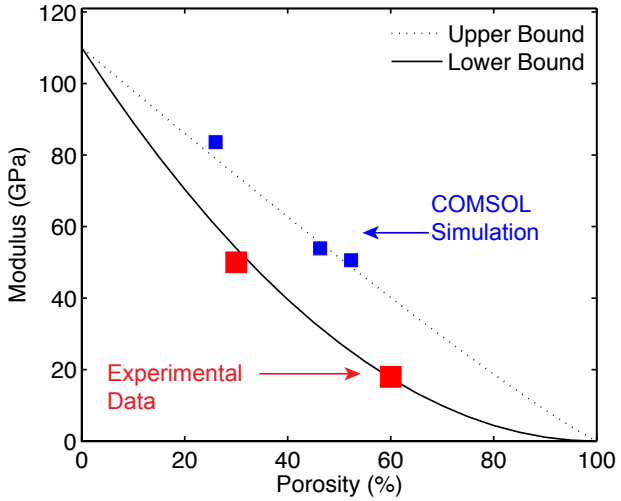

Fig.6 The prediction lines using the corrections to predict the upper bound (---) and the lower bound (—), which show the trend of decreasing mechanical modulus with a given porosity. The experimental result (■) using a microfabricated resonator technique and COMSOL simulation data (■) are shown.

EFFECTIVE THERMAL CONDUCTIVITY

The integration of a porous copper liquid transport layer to the fluidic systems reduces the thermal resistance from the liquid to the evaporation surface by adding conductive materials instead of liquids. In addition, CIOs improve the heat transfer coefficients, which can be estimated with the simple expression: $h=k/d$, where k and d are the effective thermal conductivity and pore diameter of the CIOs, respectively. This means the smaller hydraulic diameter due to smaller pore size increases the heat transfer coefficients. In addition, the smaller hydraulic diameter increases the wetting

surfaces, which improve the overall heat transfer performance of the system.

The porous copper liquid transport layer is formed on the interior surfaces of the microchannel by electrodeposition around a template of packed silica spheres. Thus, effective thermal conductivity through the microporous copper is an important input parameter for our various fluid delivery models.

By developing COMSOL models, we have investigated the thermal conductivity of CIOs. The solid matrix is copper, and void is air. Heat flux boundary condition is applied at the bottom, and this model solves the temperature distribution using heat conduction equation. The resulted temperature distribution of the porous structures is shown in Fig. 7. Based on the temperature information (T_1 and T_2) and dimentions (k and l), the thermal conductivity of the CIOs is calculated using the equation: $q''=k(T_2-T_1)/l$. The effective conductivity shows a strong dependence on the porosity. Constant porosity with varying pore sizes gives us the same effective conductivity. Three different porosities of COMSOL models are tested. COMSOL simulations indicate thermal conductivity values of ~120 W/m-K with porosity in the range of 50%, and ~ 180 W/m-K with porosity of 40%.

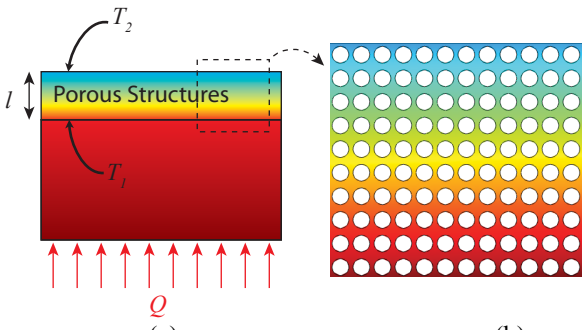

Fig.7 COMSOL Multiphysics model for predicting thermal conductivity (a) A heat flux of 5 kW/cm^2 is given at the bottom surface. The heat flux and material properties of the solid part correspond to the temperature profile. T_1 and T_2 from the simulations are used to calculate the effective conductivity of CIOs. (b) Temperature distribution through the CIOs.

COMSOL simulation results are compared with a simple approximation, as indicated in Fig. 8. Effective medium theory equations shows the conduction properties of composite media [27], [28] for a solid medium with spherical voids:

$$k_{eff} = k_f \left(1-\phi\right)^{1.5} \qquad (8)$$

where k_f is the thermal conductivity of the fluid. Effective medium theory models [29], has been agreed with Maxwell's model. Our recent experimental data using 3-omega method indicates a thermal conductivity value of 146 W/m/K for 60-75% porosity for 500 nm pore size. The details of the measurement are shown in elsewhere [22]. COMSOL simulation results, effective medium theory model and thermal measurement show a good agreement each other. Because of the relative large thermal conductivity, the integration of CIOs to the fluidic systems reduces the thermal resistance for liquid delivery to the evaporation surface.

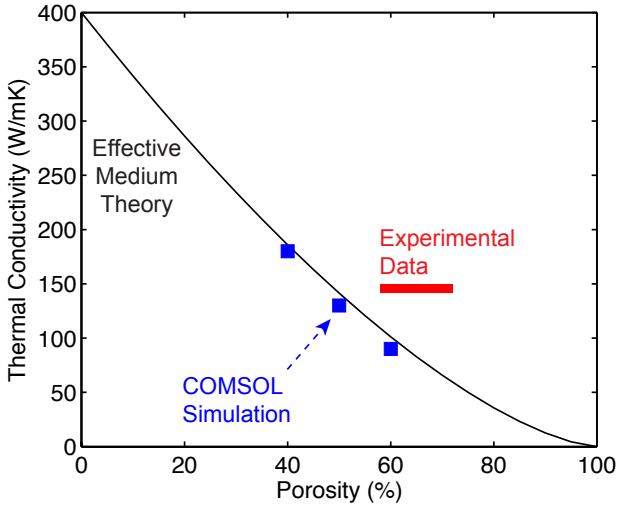

Fig.8 Thermal conductivity of CIOs with a function of porosity. Pores decrease the overall thermal conductivity of CIOs. COMSOL simulation results (■), effective medium model (—), and measured values (■) are indicated.

CONCLUDING REMARKS

We demonstrate here the mechanical and thermal characterization of CIOs by using a resonator technique and COMSOL simulations. The goal of the simulations is to illustrate the effects of those characteristics on the mechanical modulus and thermal conductivity to provide a more fundamental basis to characterize CIOs. Then, they are compared with effective medium theory to calculate the mechanical modulus and thermal conductivity, which show a good agreement. CIOs have a large range of potential applications such as interfaces between substrates, packaging materials, wicking materials, and structures of microfluidic devices. The next challenge is integration of the CIOs in real microfluid systems and observation of how the structures behave under cyclic thermal loading. Induced functional failures in the device are anticipated to most likely arise from localized failure of the attachment between nanoporous structures and substrates giving rise to local hot spots in proximity to degraded channels. Thus, the reliability and device compatibility of nanoengineered structures should be verified.

ACKNOWLEDGEMENTS

The authors would like to acknowledge financial support from DARPA (agreement # HR0011-13-2-0011, titled: Phase Separation Diamond Microfluidics for HEMT Cooling) and TOYOTA. The authors also would like to acknowledge government support under and awarded by the United States Department of Defense, Air Force Office of Scientific

Research, National Defense Science and Engineering Graduate (NDSEG) Fellowship, 32 CFR 168a.

REFERENCES

[1] D. Tuckerman and R. Pease, "High-performance heat sinking for VLSI," *IEEE Electron Device Letters*, vol. 2, no. 5, pp. 126–129, 1981.

[2] B. Agostini, M. Fabbri, J. E. Park, L. Wojtan, J. R. Thome, and B. Michel, "State of the Art of High Heat Flux Cooling Technologies," *Heat Transfer Engineering*, vol. 28, no. 4, pp. 258–281, Apr. 2007.

[3] L. Jiang, J.-M. Koo, S. Zeng, J. C. Mikkelsen, L. Zhang, P. Zhou, J. G. Santiago, T. W. Kenny, K. E. Goodson, and J. G. Maveety, "Two-phase microchannel heat sinks for an electrokinetic VLSI chip cooling system," pp. 153–157, 2001.

[4] C. H. Hidrovo, T. A. Kramer, E. N. Wang, S. Vigneron, J. E. Steinbrenner, J.-M. Koo, F.-M. Wang, D. W. Fogg, R. D. Flynn, E. S. Lee, C.-H. Cheng, T. W. Kenny, J. K. Eaton, and K. E. Goodson, "Two-Phase Microfluidics for Semiconductor Circuits and Fuel Cells," *Heat Transfer Engineering*, vol. 27, no. 4, pp. 53–63, May 2006.

[5] S. Narayanan, A. G. Fedorov, and Y. K. Joshi, "Experimental characterization of a micro-scale thin film evaporative cooling device," pp. 1–10, May 2010.

[6] S. G. Liter and M. Kaviany, "Pool-boiling CHF enhancement by modulated porous-layer coating: theory and experiment," *International Journal of Heat and Mass Transfer*, vol. 44, no. 22, pp. 4287–4311, 2001.

[7] J. A. Weibel, A. S. Kousalya, T. S. Fisher, and S. V. Garimella, "Characterization and nanostructured enhancement of boiling incipience in capillary-fed, ultra-thin sintered powder wicks," pp. 119–129, 2012.

[8] M. P. David, J. Miler, J. E. Steinbrenner, Y. Yang, M. Touzelbaev, and K. E. Goodson, "Hydraulic and thermal characteristics of a vapor venting two-phase microchannel heat exchanger," *International Journal of Heat and Mass Transfer*, vol. 54, no. 25, pp. 5504–5516, Dec. 2011.

[9] A. Tuteja, W. Choi, M. Ma, J. M. Mabry, S. A. Mazzella, G. C. Rutledge, G. H. McKinley, and R. E. Cohen, "Designing Superoleophobic Surfaces," *Science*, vol. 318, no. 5856, pp. 1618–1622, Dec. 2007.

[10] A. Ahuja, J. A. Taylor, V. Lifton, A. A. Sidorenko, T. R. Salamon, E. J. Lobaton, P. Kolodner, and T. N. Krupenkin, "Nanonails: A Simple Geometrical Approach to Electrically Tunable Superlyophobic Surfaces," *Langmuir*, vol. 24, no. 1, pp. 9–14, Jan. 2008.

[11] X. Dai, X. Huang, F. Yang, X. Li, J. Sightler, Y. Yang, and C. Li, "Enhanced nucleate boiling on horizontal hydrophobic-hydrophilic carbon nanotube coatings," *Applied Physics Letters*, vol. 102, no. 16, p. 161605, 2013.

[12] N. Miljkovic, R. Enright, and E. N. Wang, "Effect of Droplet Morphology on Growth Dynamics and Heat Transfer during Condensation on Superhydrophobic Nanostructured Surfaces," *ACS nano*, vol. 6, no. 2, pp. 1776–1785, Feb. 2012.

[13] C. Fang, M. David, A. Rogacs, and K. Goodson, "VOLUME OF FLUID SIMULATION OF BOILING TWO-PHASE FLOW IN A VAPOR-VENTING MICROCHANNEL," *Frontiers in Heat and Mass Transfer*, vol. 1, no. 1, Jun. 2010.

[14] Y. Won, Y. Gao, M. A. Panzer, S. Dogbe, L. Pan, T. W. Kenny, and K. E. Goodson, "Mechanical characterization of aligned multi-walled carbon nanotube films using microfabricated resonators," *Carbon*, vol. 50, no. 2, pp. 347–355, Feb. 2012.

[15] Y. Won, J. Lee, M. Asheghi, T. W. Kenny, and K. E. Goodson, "Phase and thickness dependent modulus of Ge2Sb2Te5 films down to 25 nm thickness," *Applied Physics Letters*, vol. 100, no. 16, p. 161905, Mar. 2012.

[16] Y. Won, Y. Gao, R. G. de Villoria, B. L. Wardle, T. W. Kenny, and K. E. Goodson, "Crust removal and effective modulus of aligned multi-walled carbon nanotube films," *Proceedings of the Thirteenth InterSociety Conference on Thermal and Thermomechanical Phenomena in Electronic Systems*, pp. 1070–1076, 2012.

[17] T. P. Bigioni, X.-M. Lin, T. T. Nguyen, E. I. Corwin, T. A. Witten, and H. M. Jaeger, "Kinetically driven self assembly of highly ordered nanoparticle monolayers," *Nature materials*, vol. 5, no. 4, pp. 265–270, Mar. 2006.

[18] R. D. Deegan, O. Bakajin, T. F. Dupont, G. Huber, S. R. Nagel, and T. A. Witten, "Capillary flow as the cause of ring stains from dried liquid drops," *Nature*, vol. 389, no. 6653, pp. 827–829, 1997.

[19] J. J. Razink and N. E. Schlotter, "Correction to 'Preparation of monodisperse silica particles: Control of size and mass fraction' by G.H. Bogush, M.A. Tracy and C.F. Zukoski IV, Journal of Non-Crystalline Solids 104 (1988) 95–106," *Journal of Non-Crystalline Solids*, vol. 353, no. 30, pp. 2932–2933, Oct. 2007.

[20] G. H. Bogush, M. A. Tracy, and C. F. Zukoski, "Preparation of monodisperse silica particles: control of size and mass fraction," *Journal of Non-Crystalline Solids*, vol. 104, no. 1, pp. 95–106, 1988.

[21] W. Stöber, A. Fink, and E. Bohn, "Controlled growth of monodisperse silica spheres in the micron size range," *Journal of colloid and interface science*, vol. 26, no. 1, pp. 62–69, 1968.

[22] M. T. Barako, T. Dussealt, M. Asheghi, and K. E. Goodson, "Thermal Conduction in Nanoporous Copper Inverse Opal," Proceedings of the Fourteen InterSociety Conference on Thermal and Thermomechanical Phenomena in Electronic Systems, Mar. 2014.

[23] M. Panzer, G. Zhang, D. Mann, X. Hu, E. Pop, H. Dai, and K. Goodson, "Thermal Properties of Metal-Coated Vertically Aligned Single-Wall Nanotube Arrays," *Journal of Heat Transfer*, vol. 130, p. 052401, 2008.

[24] S. H. Park, D. Qin, and Y. Xia, "Crystallization of mesoscale particles over large areas," *Advanced Materials*, vol. 10, no. 13, pp. 1028–1032, 1998.

[25] J. Kováčik, "Correlation between Young's modulus and porosity in porous materials," *Journal of materials science letters*, vol. 18, no. 13, pp. 1007–1010, 1999.

[26] A. P. Roberts and E. J. Garboczi, "Elastic properties of

model porous ceramics," *J. Am. Ceram. Soc.*, vol. 83, no. 12, pp. 3041–3048, 2000.
[27] J. C. Maxwell, *A Treatise on Electricity and Magnetism*. 1892.
[28] H. T. Aichlmayr and F. A. Kulacki, "A Transient Technique for Measuring the Effective Thermal Conductivity of Saturated Porous Media With a Constant Boundary Heat Flux," *Journal of Heat Transfer*, vol. 128, no. 11, p. 1217, 2006.
[29] S. Datta, C. T. Chan, K. M. Ho, and C. M. Soukoulis, "Effective dielectric constant of periodic composite structures," *Phys. Rev. B*, vol. 48, no. 20, p. 14936, 1993.